Nanoscale

Accepted Manuscript

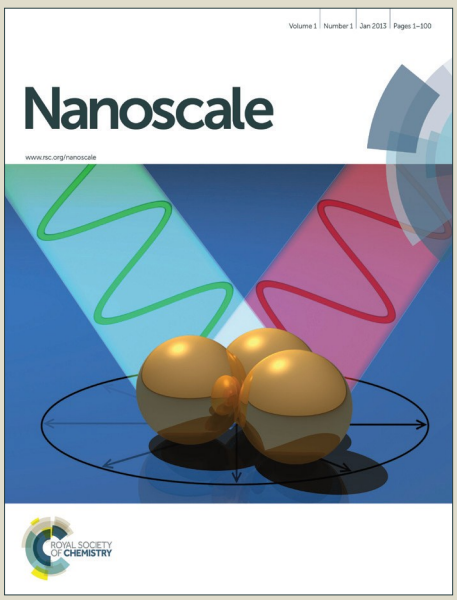

ROYAL SOCIETY OF CHEMISTRY

www.rsc.org/nanoscale

Journal Name

RSCPublishing

ARTICLE

Controllable Synthesis of Mesoporous Carbon Nanospheres and Fe-N/Carbon Nanospheres as Efficient Oxygen Reduction Electrocatalysts

Cite this: DOI: 10.1039/xoxxoooooox

Received ooth January 2012,
Accepted ooth January 2012

DOI: 10.1039/xoxxoooooox

www.rsc.org/

Jing Wei,[a] Yan Liang,[a] Xinyi Zhang,[b] George P. Simon,[c] Dongyuan Zhao,[ad] Jin Zhang,[e] Sanping Jiang,[e] Huanting Wang*[a]

The synthesis of mesoporous carbon nanospheres (MCNs), especially with diameters below 200 nm remains a great challenge due to weak interactions between the carbon precursors and soft templates, as well as the uncontrollable cross-linking rate of carbon precursors. Herein, we demonstrate a simple acid-assisted, hydrothermal synthesis approach to synthesizing such uniform MCNs with well controlled diameters ranging from 20 to 150 nm under highly acidic conditions (2 M HCl). Both carbon precursor and template are partly protonated under such conditions and show additional Coulombic interactions with chloride ions (acts as mediators). This kind of enhanced interaction is similar to that of the "$I^+X^-S^+$" mechanism in the synthesis of mesoporous metal oxide, which can effectively retard the cross-linking rate of resol molecules and avoid macroscopic phase separation during the hydrothermal synthesis. Due to their uniform spherical morphology, small diameter, and high surface areas, MCNs can be modified with Fe and N species via impregnation of cheap precusors (ferric nitrate and dicyandiamide), which are further converted into nonprecious electrocatalysts for oxygen reduction reation. The resulting Fe-N/MCNs exhibit high catalytic activities, long-term stability and improved methanol tolerance in alkaline conditions, which can be potentially used in direct methanol fuel cells and metal-air batteries.

Introduction

Nanoporous carbon nanospheres have received considerable attention due to their potential applications in adsorption, separation, catalysis, drug delivery and energy storage/conversion.[1-14] In particular, mesoporous carbon nanospheres (MCNs) with a high surface area, an open framework, and large pore size can further enhance their performance in various applications involved in the transport of large guest molecules.[15-33] Many attempts have been made to prepare MCNs via a hard-templating method, in which a carbon precursor is induced into the mesopores of silica nanospheres or colloidal crystals by impregnation, followed by *in-situ* carbonization and removal of the silica using a hot alkali solution or hydrofluoric acid.[34-39] However, the hard-templating method is time-consuming and costly. More importantly, the pore size, mesostructure and morphology of MCNs replica are difficult to adjust due to a limited choice of appropriate hard templates.

The soft-templating method has recently been intensively investigated to prepare mesoporous carbons with various mesostructures, framework components, and morphologies, as well as tuneable pore sizes.[40-46] In the soft-templating method, the mesostructure is formed via organic-organic self-assembly process due to the hydrogen bonding between carbon precusor (i.e. phenolic-formaldehyde resin) and template (i.e. triblock copolymer Pluronic F127; $EO_{106}PO_{70}EO_{106}$; EO, ethylene oxide; PO, propylene oxide). By using this soft-templating method, mesoporous carbons usually form either films, monoliths or particles with micrometer size.[47] Hydrothermal synthesis has been widely used to prepare polymer (or carbon) spheres. It is reasonable to combine the organic-organic self-assembly process and hydrothermal synthesis to obtain MCNs. However, it is still a challenge to produce such spheres due to the difficulty to simultaneously control the cross-linking rate of carbon precursors and self-assembly process of precursors and templates. During the hydrothermal process, the fast cross-linking rate of carbon precursors needs to match the strong interactions between template and carbon precusors because otherwise, the excessive cross-linking of the carbon precusors would lead to macroscopical phase separation of carbon precursors and templates. More recently, Zhao and co-workers for the first time reported a low-concentration hydrothermal route to synthesize MCNs with an uniform particle size (20–140 nm), which indicates the feasibility of preparing MCNs under a hydrothermal treatment.[22] In this method, a multi-step procedure using dilute micelles/resol solution at very low concentration (i.e. F127, 10^{-7} mol/L) is used prior to a

hydrothermal treatment. The use of such a low concentration decreases the cross-linking rate so as to match the weak interactions between the carbon precusor and template. In addition, most of the examples for synthesis of mesoporous carbon nanospheres were under alkline conditions. The template molecules and carbon precursor only show weak hydrogen-bonding interaction. Dai and co-workers have demonstrated the synthesis of ordered mesoporous carbon using phloroglucinol (or resorcinol)-formaldehyde as a carbon source, block copolymer (F127) as a template in highly acidic condition via enhanced hydrogen-bonding interaction by using the "$I^+X^-S^+$" mechanism, which was used to prepare mesoporous metal oxides.[41, 48-49] However, it is challenging to control the morphology of mesoporous carbon such as nanospheres, due to the rapid polymerization of the carbon source (phloroglucinol or resorcinol/formaldehyde) under strongly acidic conditions. As far as we known, mesoporous carbon nanospheres are rarely prepared in acidic conditions via enhanced hydrogen-bonding interaction.

Herein we demonstrate a simple acid-assisted organic-organic self-assembly approach to synthesize uniform MCNs via direct hydrothermal treatment of phenol-formaldehyde resol and triblock copolymer Plurnonic F127 under highly acidic conditions (2 M HCl), followed by a carbonization process. Both the resol and F127 are partly protonated under highly acidic conditions and thus show an enhanced hydrogen-bonding interaction via Coulombic interactions with Cl^- (as a mediator). This kind of enhanced interaction is similar to that of the "$I^+X^-S^+$" mechanism in the synthesis of mesoporous metal oxides, which can retard the cross-linking rate of the resol molecules trapped in the triblock copolymer micelles and thus avoid macroscopic phase separation during the hydrothermal synthesis. The MCNs show a high surface area (596 m^2/g), large pore volume (0.77 cm^3/g) and a well controllable diameter ranging from 20 to 150 nm, simply by changing the mass ratio of template to resol. Due to their uniform spherical morphology, small diameter, nanoporous structure and high surface area, MCNs can be modified with Fe and N species via impregnation of cheap precusor (ferric nitrate and dicyandiamide), which are further converted into nonprecious electrocatalysts for oxygen reduction. This kind of Fe-N/MCNs exhibits high catalytic activity, long-term stability and excellent methanol tolerance in alkaline conditions.

Experimental

Chemicals: All the chemicals were purchased from Sigma-Aldrich Australia without further purification.

Synthesis of mesoporous carbon nanospheres (MCNs): For the typical synthesis of the mesoporous carbon nanospheres, F127 (0.2 g) was dissolved in 2 M HCl aqueous solution (50 mL) at room temperature, followed by the addition of 1.2 g of 20 wt% resol solution (in ethanol). After being stirred for 10 min, the solution was transfer to a Teflon-lined autoclave (100 mL) for hydrothermal treatment at 120 °C for 12 h. The polymer spheres were recovered by centrifugation and dried at 60 °C in an oven. The yield was about 61 %. The mesoporous carbon nanospheres were obtained by carbonization at 700 °C for 3 h at a heating rate of 1 °C/min in Ar atmosphere. To adjust the particles size, 0.30, 0.25, 0.18, and 0.15 g of F127 were used, respectively, while the amounts of resol and solvent were fixed. The resulting mesoporous carbons were denoted as MCN-x, where x refers the mass ratio of template to resol.

Preparation of Fe-N-MCNs: The as-made polymer spheres were calcined at 350 °C in Ar to remove F127 and get MCN-350. 5 g of MCN-350 was dispersed in 30 mL of ethanol solution containing 0.25 g of ferric nitrate nonahydrate via sonication. After ethanol evaporation, Fe loaded MCN was obtained. The resulting powder was ground with dicyandiamide at a mass ratio of 1:2 and heated to 700 °C for 2 h in Ar atmosphere. After cooling down to room temperature, Fe-N/MCN was prepared. When the carbonization temperature was changed to 600 or 800 °C, the corresponding samples were denoted as Fe-N/MCN-600 or Fe-N/MCN-800. For comparison, the sample without Fe loading (MCN-350) were also mixed with dicyandiamide, and carbonized; the resulting sample was denoted as N-MCN.

Characterization: Scanning electron microscopy (SEM) images were taken with a field-emission scanning electron microscope (FEI Nova NanoSEM 450) operating at 5 kV. For the polymer nanospheres, the sample was sputter-coated with platinum prior to SEM examination. For the carbon nanospheres, the sample was directly spread on a carbon tape. Transmission electron microscopy (TEM) images were taken by a JEOL 2100F FEG TEM (Japan) and a FEI Tecnai G2 T20 operated at an accelerating voltage of 200 kV. The samples were first dispersed in ethanol; a drop of the dispersion was then added to a copper grid with holey carbon film and dried, prior to TEM characterization. Nitrogen adsorption/desorption isotherms were measured at -196 °C with a Micromeritics ASAP 2010 analyzer. Before measurement, the samples were degassed in a vacuum at 180 °C for at least 8 h. The Brunauer-Emmett-Teller (BET) method was used to calculate the specific surface area by using the adsorption data at p/p_0 range of 0.05 ~ 0.25. The pore size distribution was derived from the adsorption branch by using the nonlocal density functional theory (NLDFT) model method. The total pore volume was estimated from the adsorbed amount at a p/p_0 value of 0.995. The Raman spectra was measured on WITEC Alpha 300 confocal micro-Raman system equipped with a 532 nm laser source and 100X objective lens. X-ray photoelectron spectroscopy (XPS) experiments were carried out on a Kratos AXIS Ultra DLD system with Al Kα radiation as X-ray source for radiation. Powder X-ray diffraction (PXRD) patterns were recorded in the 2θ range of 10 − 90 ° at room temperature using a Miniflex 600 diffractometer (Rigaku, Japan) in transmission geometry using Cu Kα radiation (15 mA and 40 kV) at a scan rate of 2 °/min and a step size of 0.02°.

Electrochemical measurements. Cyclic voltammetry (CV) and linear sweep voltammetry (LSV) voltammetry were performed by using a μAutolab electrochemical analyzer in a conventional three-electrode electrochemical cell. A Pt wire auxiliary electrode, a saturated Ag/AgCl (saturated with 3 M KCl) reference electrode, and rotating disk working electrode were used. For oxygen reduction reaction (ORR), 10 mg of Fe-N/MCN materials (or commercial Pt/C, 20 wt%, from Sigma-Aldrich) was dispersed in 2.4 mL of ethanol and 0.1 mL of 5.0 wt % Nafion solution under ultrasonication to form an electrocatalyst ink. Then 20 μL (or 5 μL for Pt/C) of the electrocatalyst ink was dropped on the surface of the pre-cleaned rotating disk electrode (5 mm diameter, 0.196 cm^2) and dried at room temperature. A 0.1 M KOH solution was used as the electrolyte for all the CV and RDE studies. Argon and O_2 were used to achieve oxygen-free and oxygen-rich environments. The electrolyte was saturated with Ar (or O_2) before test. The CV curves were recorded at a scan rate of 50 mV/s; the RDE curves were recorded at a scan rate of 10 mV/s.

A flow of O_2 was maintained over the electrolyte during the CV and LSV test to ensure O_2 saturation. The numbers of electrons transferred (n) during ORR was calculated by Koutecky-Levich equation, at various electrode potentials:

$$\frac{1}{J} = \frac{1}{J_L} + \frac{1}{J_K} = \frac{1}{B\omega^{0.5}} + \frac{1}{J_K}$$

$$B = 0.62nFC_0D_0^{2/3}v^{-1/6}$$

where J is the measured current density, J_K and J_L are the kinetic and diffusion-limiting current densities, respectively, ω is the angular velocity, n is transferred electron number, F is the Faraday constant (96485 C mol^{-1}), C_0 is the bulk concentration of O_2 (1.2×10^{-6} mol cm^{-3}), D_0 is the diffusion coefficient of O_2 in 0.1 M KOH (1.9×10^{-5} cm^2 s^{-1}), and ν is the kinematic viscosity of the electrolyte (0.01 cm^2 s^{-1}).

Results and Discussion

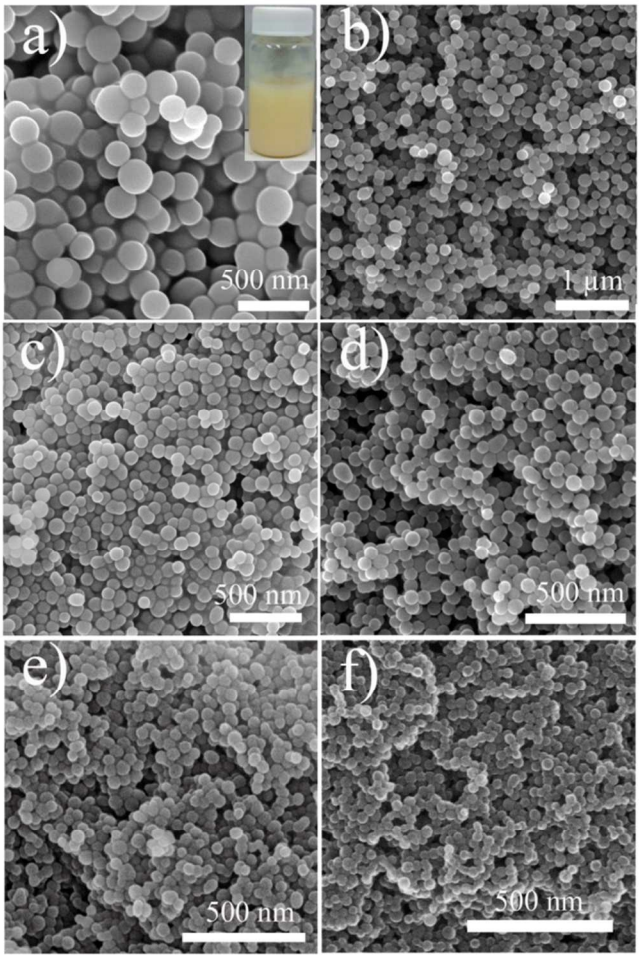

Figure 1 Scanning electron microscopy (SEM) images of the polymer nanospheres before carbonization (a, c, e) and the corresponding mesoporous carbon nanospheres synthesized with different mass ratios of F127 to resol: b) MCN-0.9; d) MCN-1.0; f) MCN-1.25. The inset in a) is an optical image of polymer spheres in an aqueous solution.

After direct hydrothermal treatment of resol and F127 dissolved in 2 M HCl solution at 120 °C, a stable suspension of light-yellow polymers was obtained, indicating that the polymer nanospheres are well dispersed in water (Figure 1a, inset). Scanning electron microscopy (SEM) image of the polymer nanospheres prepared at a mass ratio of the template to resol of 0.9 (denoted as-made MCN-0.9) shows a uniform spherical morphology with a diameter of around 200 nm (Figure 1a). After the removal of the Pluronic F127 templates and conversion of phenolic-formaldehyde resin to carbon framework at 700 °C in Ar, the uniform spherical morphology is well maintained, revealing a good framework stability of the template/phenolic-formaldehyde resin composites (Figure 1b). The diameter of the spheres is around 120 nm, as estimated from the SEM images, which is much smaller than that of the parent polymer spheres (200 nm) due to a severe shrinkage (~ 40 %) during the carbonization process. When the mass ratio of the template to resol increases to 1.0, as-made MCN-1.0 still shows a spherical morphology but with a decreased diameter of about 100 nm (Figure 1c). After the carbonization, the diameter of the carbon spheres MCN-1.0 decreases to about 60 nm (Figure 1d). When the mass ratio of template to resol further increases to 1.25, and both polymer and corresponding carbon nanospheres (MCN-1.25) show decreased diameters of 50 and 30 nm, respectively (Figure 1e, and f). Further increases the mass ratio to 1.5 results in ultrasmall carbon nanoparticles (Figure S1a). In addition, a much lower mass ratio of the template to resol (0.75) was used to investigate its effect on the size of carbon spheres, and only large spheres with micrometer sizes were obtained (Figure S1b). As the concentrations of both F127 and resol were increased by a factor of three (i.e. F127, 9.5×10^{-4} mol/L), mesoporous carbon nanospheres were still obtained (Figure S2); whereas further increasing the concentration of F127 and resol by a factor of five led to a mixture of carbon microspheres and nanospheres, implying that a very high concentration of the precursor and template resulted in excessive cross-linking of the carbon precursor to form microspheres. When the acid concentrations decreased to 0.1 M, carbon spheres with diameters of several micrometres were synthesized (Figure S3). When the acid concentration increased to 5 M, very small carbon particles (~ 20 nm) were obtained, showing that a higher acidity led to smaller carbon spheres.

Transmission electron microscopy (TEM) images of mesoporous carbon nanospheres (MCN-0.9) show a uniform spherical morphology with a diameter of about 120 nm, consistent with SEM results (Figure 2a, b). The mesoporous and microporous framework can be readily observed on a high resolution TEM image, where the mesopores were generated by removing the F127 micelles formed during the self-assembly process, while the micropores were produced by small gas molecules (i.e. CO_2, H_2O) escaping from the phenolic formaldehyde resin during the carbonization. The TEM image of the MCN-1.0 also shows a spherical morphology and mesoporous structure but with a decreased diameter, which agrees well with SEM results (Figure 2c). With further increasing the mass ratio of template to resol, a decreased diameter is observed, as shown in the TEM image of MCN-1.25. However, in this case the spheres with small diameters are not uniform and the particles tend to aggregate to decrease the surface energy (Figure 2d). To further determine the porosity of the MCN, MCN-0.9 was characterized by using a N_2 sorption technique; its N_2 sorption isotherm shows pseudo-type-I curve with a H_1 hysteresis, corresponding to the microporous and

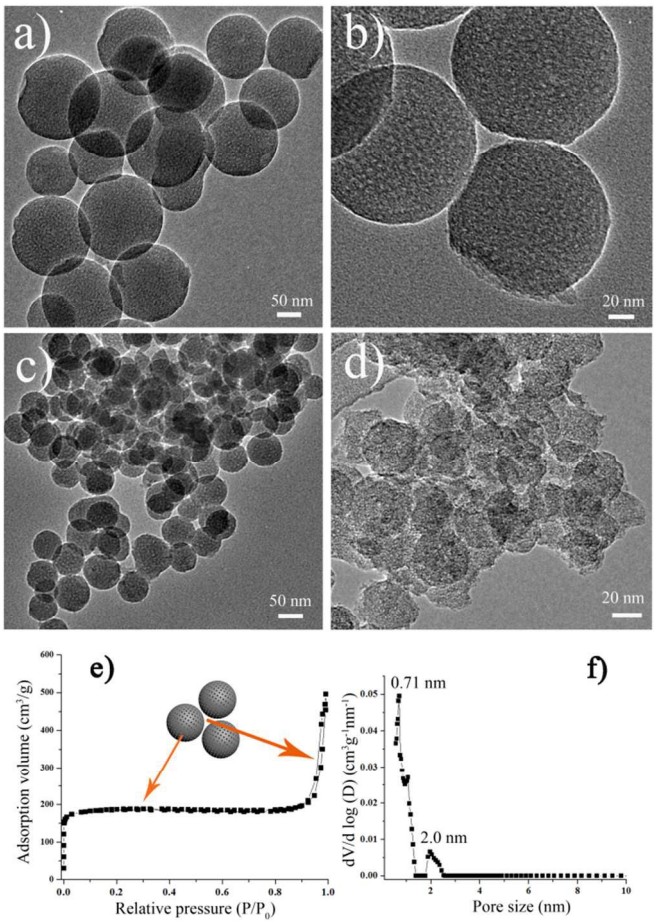

Figure 2 Transmission electron microscopy (TEM) images of mesoporous carbon nanospheres (MCNs) synthesized with different mass ratios of F127 to resol: a, b) MCN-0.9, c) MCN-1.0, and d) MCN-1.25. N_2 sorption isotherms (e) and nonlocal density functional theory (NLDFT) pore size distributions (f) of typical mesoporous carbon nanospheres (MCN-1.0).

mesoporous structure (Figure 2e). Additionally, a large hysteresis loop at a high relative pressure (0.95) reveals the existence of large pores, which is attributed to the packing of nanospheres. The pore size distributions are derived using the nonlocal density functional theory (NLDFT) model, and show a uniform micropore size of 0.71 nm and a mesopore size of 2.0 nm, consistent with the TEM results (Figure 2f). The pore size is smaller than that of conventional mesoporous carbon prepared using EISA method,[40] mainly due to a large shrinkage during the carbonization. The Brunauer-Emmett-Teller (BET) surface area and pore volume are 596 m^2/g and 0.77 cm^3/g, respectively.

On the basis of the above results, we propose an acid-assisted organic-organic self-assembly mechanism to explain the formation of MCNs. The low activity carbon precursor resol, which is different from the commonly used phloroglucinol or resorcinol/formaldehyde resin, demonstrates a controllable polymerization rate under a highly acidic condition; both PEO segment of F127 and resol are partially pronated, resulting in an additional Coulombic interaction with negatively charged Cl^- anions in the solution, and enhanced interactions. During the hydrothermal process, the cross-linking of resol induces the self-assembly of resol and F127, where the triblock copolymers (F127) form spherical micelles with a PPO core and PEO shell. The resol molecules are trapped in the region of PEO segment of block copolymer micelles due to their enhanced interaction (Figure 3, Step 1). With further cross-linking of resol, the resol/F127 composite micelles further aggregate, connected with each other through carbon-carbon bonds to form nanospheres with a low surface energy (Figure 3, Step 2). During the carbonization process, the template decomposes due to its low thermal stability, while the phenol-formaldehyde resin further cross-links and converts to a carbon framework (Figure 3, Step 3). Due to strong interactions of template micelles and resol, the resol molecules are trapped in the template micelles, which can avoid the excessive cross-linking of resol molecules from different composite micelles. Our method can be used to prepare mesoporous carbon nanospheres at much higher concentrations (F127, 9.5×10^{-4} mol/L, almost a factor of 10^4 times) than those in the typical low concentration synthesis (10^{-7} mol/L).[22] As the concentration of F127 is further increased to 1.6×10^{-3} mol/L, the excessive cross-linking of resol in adjacent composite micelles can occur and result in a mixture of microspheres and nanospheres. When the mass ratio of template to resol increases, more resol molecules become trapped in the template micelles and the cross-linking rate of resol decreases, leading to a smaller particle size. A higher acidic environment leads to highly pronated resol and triblock copolymers, and thus can effectively retard the cross-linking rate of resol and form smaller carbon spheres.

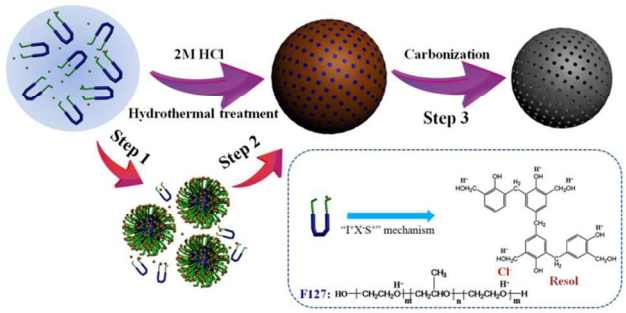

Figure 3. Schematic illustration of the formation of uniform mesoporous carbon nanospheres (MCNs) using resol as a carbon precursor, triblock copolymer Pluronic F127 as a template, 2M hydrochloric acid as a solvent via an acid assisted organic-organic self-assembly process: Step 1: the polymerization of resol induces the phase separation of F127 to form spherical micelles with PPO core and PEO shell, where the resol is located in the PEO shell due to the strong Coulombic interactions between the protonated resol and PEO via the $I^+X^-S^+$ mechanism; Step 2: the further polymerization of resol induces the aggregation of composited spherical micelles to polymer nanospheres; and Step 3: carbonization under inert atmosphere to selectively remove F127 and form carbon framework.

The oxygen reduction reaction (ORR) is important for energy conversion devices such as fuel cells and metal-air batteries.[50-55] Due to the sluggish kinetics of ORR, Pt and Pt-based materials are proved to be the best electrocatalysts in these systems. However, the high cost, poor long-term stability and scarcity of Pt hinders their large-scale application and thus the commercialization of fuel cells. Recently, nitrogen-doped carbon, as well as non-precious metal oxide and carbides have been proved to possess good ORR performance.[50-56] The doping N atoms can disrupt the electroneutrality of adjacent

carbon atoms and create positively charged sites favourable for oxygen adsorption and reduction. The incorporation of transition metal oxide and carbides into the N-doped carbon can further increase the ORR performance.[56] In our study, MCNs with high surface area, uniform spherical morphology, good conductivity and chemical stability, are further investigated as an ORR electrocatalyst support. To configure a high-performance electrocatalyst for ORR, the cheap precursors, $Fe(NO_3)_3$ and dicyandiamide were used as Fe and N source, respectively. After incorporation of Fe and N sources into the mesoporous polymer nanospheres (prepared via the calcination of as-made MCN at 350 °C in Ar to remove F127), the composite nanospheres were annealed at a high temperature (i.e. 700 °C) to obtain Fe-N/MCNs.

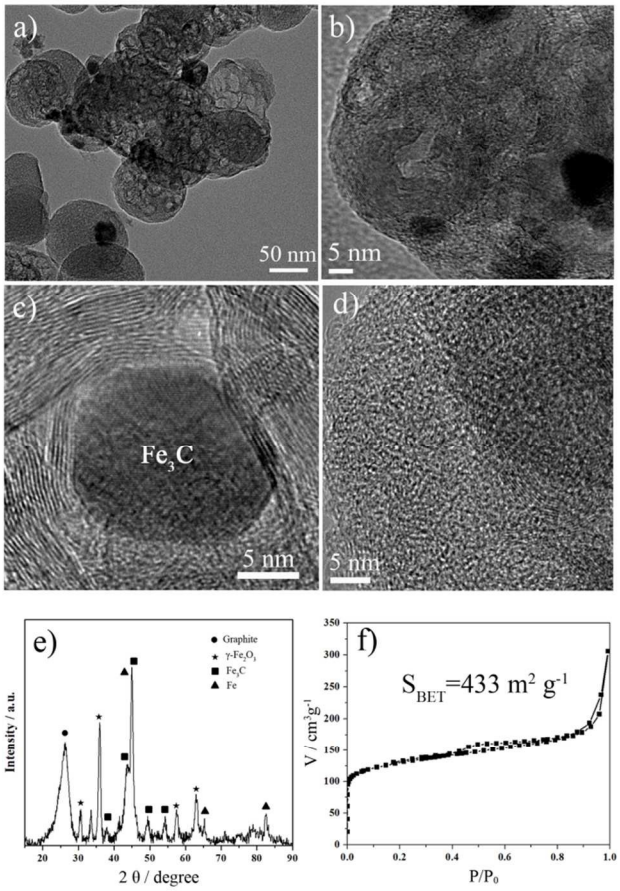

Figure 4 a-d) TEM images of Fe-N/MCNs with different magnifications; e) XRD patterns and f) N_2 sorption isotherms of Fe-N/MCNs calcined at 700 °C in Ar atmosphere.

SEM images of Fe-N-MCNs show a similar spherical morphology to MCNs (Figure S4). TEM images reveal that Fe-based nanoparticles are embedded in carbon spheres, indicating that the Fe species were successfully loaded into the porous carbon nanospheres (Figure 4a). During the carbonization, the Fe species dispersed in the carbon matrix played two roles: catalyzing the graphitization and acting as a template for formation of the graphitic structure.[57] The Fe species migrated to form large Fe/Fe_3C nanocrystals, resulting in some cavities. Hence Fe-N-MCNs have larger pore sizes than primitive MCNs (Figure 4b). Fe_3C nanoparticles were also formed, and wrapped up by a graphite layer (Figure 4c). In contrast, the carbon without Fe catalyst shows an amorphous structure, similar to the unmodified carbon sphere (Figure 4d). XRD patterns confirm the existence of Fe, Fe^3C and γ-Fe_2O_3 phase in the carbon material (Figure 4e). The BET surface area and pore volume of Fe-N/MCNs calculated from the N2 sorption isotherms are 434 m^2/g and 0.47 cm^3/g, respectively. The high surface area of the catalyst means that more active sites are exposed, and the mass transport is enhanced, which is beneficial to a high catalytic performance.

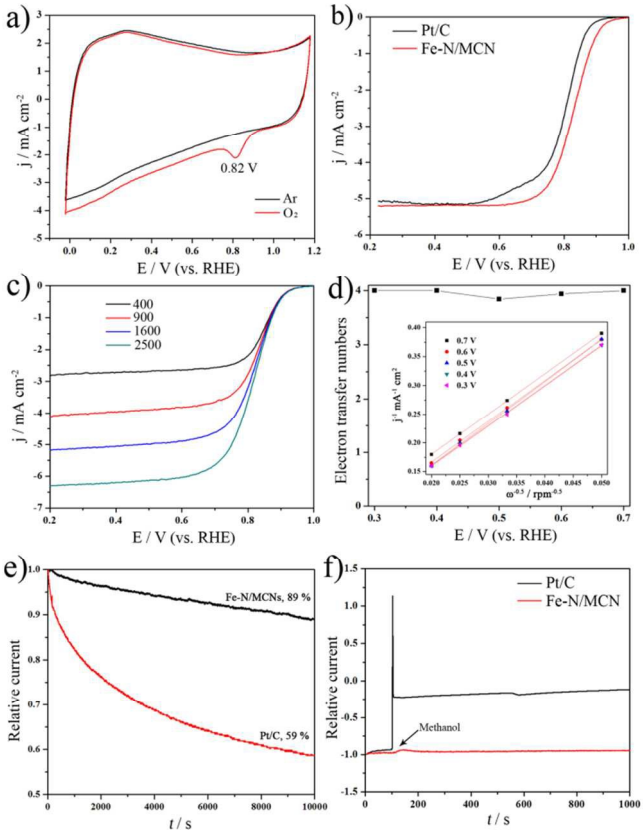

Figure 5 ORR performance of Fe-N/MCNs: a) CV curves in Ar and O_2 saturated 0.1 M KOH solution; b) LSV curves of commercial Pt/C and Fe-N/MCNs at 1600 rpm in O_2 saturated 0.1 M KOH solution; c) LSV curves of Fe-N/MCNs at different rotating speeds; d) electron transfer numbers of the catalysis from 0.3 to 0.7 V; inset in d) is K-L plots for Fe-N/MCNs from 0.3 to 0.7 V. e) Current-time chronoamperometric response of Pt/C and Fe-N/MCNs at 0.83 V in O_2-saturated 0.1 M KOH solution. f) Chronoamperometric response of Pt/C and Fe-N/MCNs at 0.83 V in O_2-saturated 0.1 M KOH solution. The arrow indicates the introduction of 4 vol% methanol.

The electrocatalytic ORR activity of Fe-N/MCNs was evaluated using cyclic voltammetry and a rotating disk electrode (RDE). The CV curves of Fe-N/MCNs were recorded in Ar or O_2 saturated 0.1 M KOH solution at a scan rate of 50 mV/s (Figure 5a). For Ar saturated solution, featureless voltammetric currents were observed for Fe-N/MCNs. By contrast, for O_2 saturated solutions, Fe-N/MCNs exhibited a cathodic ORR peak at 0.82 V, which indicates a good ORR activity. The linear sweep voltammetry (LSV) curves show that the onset potentials of Fe-N/MCNs and commercial Pt/C (20 wt%, Sigma-Aldrich) are 0.95 and 0.91 V, respectively, and the half-wave potentials of Fe-N/MCNs and commercial Pt/C are 0.83 and 0.80 V, respectively (Figure 5b). The limiting current densities of both Fe-N/MCNs and commercial Pt/C are about

5.2 mA cm^{-2}, which indicates a high catalytic activity of Fe-N/MCMs. Such a high catalytic performance is attributed to their high surface area, and small diameters of carbon spheres, which provide easy access to the active sites and enhanced mass-transport properties. To determine the electron transfer numbers, a set of LSV curves were recorded from 400 to 2500 rpm in O_2 saturated 0.1 M KOH at a scan rate of 10 mV s^{-1} (Figure 5c). The Koutecky-Levich (K-L) plots derived from Figure 5c show a good linearity and parallelism over the entire potential range (0.3 - 0.7 V), which indicates that their electron transfer numbers for ORR are similar (Figure 5d). The electron transfer numbers calculated from K-L equation are near 4 over the entire potential range, suggesting that the electrocatalysis exhibits a dominant four-electron oxygen reduction process (Figure 5d inset). The stability of Fe-N/MCNs and commercial Pt/C was assessed with chronoamperometirc measurements at 0.83 V. After 10000 s of reaction, the loss of current density is 11 % for Fe-N/MCNs and 41% for commercial Pt/C, respectively, indicating that our materials show higher stability than Pt/C material (Figure 5e).

It is well known that the possible crossover of methanol from anode to cathode causes the poisoning of Pt catalyst in the cathode, which inevitably reduces the reduction current. It's thus necessary to investigate the electrocatalytic selectivity of Fe-N/MCNs against the electrooxidation of methanol molecules. For the Fe-N/MCNs, the ORR current did not change after methanol was added in the 0.1 M KOH solution saturated with O_2 (Figure 5f). For comparison, the corresponding current of Pt/C shifted from a cathodic current to a reversed anodic current in a very short time after the methanol addition. The results indicate that Fe-N/MCNs shows a better methanol tolerance, and are thus a promising cathode catalyst for alkaline direct methanol fuel cells.

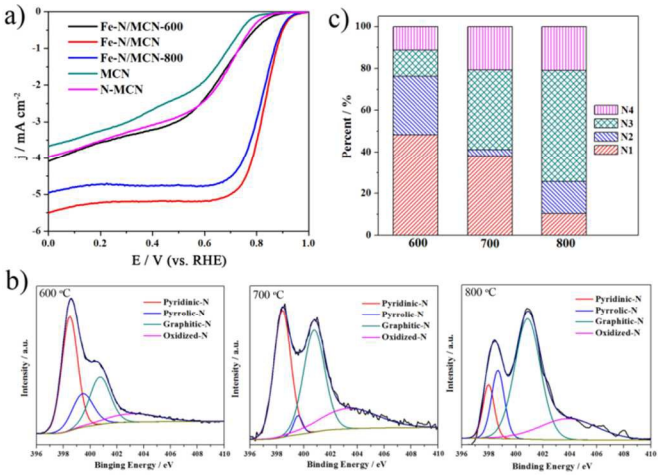

Figure 6 Fe-N/MCNs with different carbonization temperature (600, 700 and 800 °C): a) LSV curves at 1600 rpm in O_2 saturated 0.1 M KOH solution; b) N 1s XPS spectrum and c) the contents of different N groups calculated from N 1s XPS spectrum: N1, pyridinic-N; N2, pyrrolic-N; N3, graphitic-N; N4, Oxidized-N.

To address the possible mechanism for the high catalytic activity of Fe-N/MCNs, N doped MCNs without Fe modification were also prepared (denoted as N-MCN). MCNs show a low onset potential and limiting current density (Figure 6a). After N doping, the onset potential and limiting current density are slightly improved, because the doped N atoms can break the electroneutrality of nanocarbons to create charged sites favourable for O_2 adsorption. After modification of N and Fe in MCNs, both the onset potential and limiting current density increase dramatically, demonstrating that the modification of Fe is important to increase the catalytic activity. The Fe species can not only create new catalytic sites (Fe-N/C), but also act as a graphitization catalyst during carbonization, promoting the formation of highly graphitic carbon and thus increasing the conductivity of subsequent carbon material. Carbonization temperature is also important to the ORR performance since the temperature affects the degree of graphitization and N doping mode. The Fe and N co-modified materials calcined at 600 and 800 °C (denoted as Fe-N/MCN-600 and Fe-N/MCN-800) were also used as ORR catalysts. From LSV curves, Fe-N/MCN-600 shows a lower onset potential and limiting current density than Fe-N/MCNs (calcined at 700 °C); whereas Fe-N/MCN-800 exhibits a similar onset potential and a little lower limiting current density than Fe-N/MCNs. The degree of graphitization generally increases as the carbonization temperature increases from 600 to 800 °C as shown by XRD patterns and Raman spectra (Figure S5). The lower performance of Fe-N/MCN-600 may result from its lower degree of graphitization, which leads to a low conductivity and thus restricts electron transfer during oxygen reduction reaction and reduces the electrocatalytic activity. For Fe-N/MCN-800, the slightly inferior performance may result from the loss of catalytic sites (i.e. N, Fe) at a high temperature. Fe-N/MCNs carbonized at 700 °C shows best performance due to balanced graphitic degree and active sites. Elements analysis results reveal that N contents in Fe-N/MCN-600, Fe-N/MCN (700 °C) and Fe-N/MCN-800 are 18.9, 6.0 and 2.2 wt %, respectively. From XPS results, Fe-N/MCNs possess high contents of pyridinic and graphitic N, which may be important to the onset potential and limiting current density (Figure 6). For comparison, Fe-N/MCNs-600 has a low content of graphitic N and a high content of inactive pyrrolic N, which has little effect on the electrochemical performance. Fe-N/MCNs-800 has less pyridinic N and more inactive pyrrolic N. The XPS results further explain the good performance of Fe-N/MCNs catalysts.

Conclusions

In summary, we have demonstrated a simple, acid-assisted organic-organic self-assembly approach to synthesize uniform MCNs with a high surface area, large pore volume and well controlled diameter ranging from 20 to 150 nm via direct hydrothermal treatment of resol and triblock copolymer under highly acidic conditions followed by a carbonization process. The highly acidic solvent is pivotal to the self-assembly process due to the enhanced interaction between protonic carbon precursors and templates via the "$I^+X^-S^+$" mechanism. Such enhanced interactions between template and carbon precursor may be extended to the synthesis of mesoporous nanospheres with a various compositions via a direct hydrothermal route. Additionally, MCNs might be easily extended to a large scale synthesis, due to a high concentration of template and resol (i.e. F127: 9.5×10^{-4} mol/L). The mesoporous carbon nanospheres can be further modified with Fe and N species due to their porous structure and high surface area, which show high performance as a nonprecious electrocatalyst for oxygen reduction reaction. In addtion, it is believed that the mesoporous carbon nanospheres have great potential for use as

high performance sorbents, catalyst supports, drug delivery carriers and energy storage materials.

Acknowledgements

J. Wei and Y. Liang contributed equally to this work. This work is supported by the Australian Research Council (Discovery Project No. DP150100765). The authors thank the staff of Monash Centre for Electron Microscopy for their technical assistance in SEM and TEM.

Notes and references

[a]New Horizons Research Center and Department of Chemical Engineering, Monash University, Clayton, Victoria 3800, Australia.
[b]School of Chemistry, Faculty of Science, Monash University, Clayton, Victoria 3800, Australia.
[c]New Horizons Research Center and Department of Materials Engineering, Monash University, Clayton, Victoria 3800, Australia.
[d]Department of Chemistry, Fudan University, Shanghai, P. R. China.
[e]Fuels and Energy Technology Institute & Department of Chemical Engineering, Curtin University, Perth, WA 6102, Australia.
*Corresponding author. E-mail: huanting.wang@monash.edu
Electronic Supplementary Information (ESI) available: [details of any supplementary information available should be included here]. See DOI: 10.1039/b000000x/

1. A.-H. Lu, G. P. Hao, Q. Sun, *Angew. Chem. Int. Ed.* **2011**, *50*, 9023.
2. A.-H. Lu, T. Sun, W. C. Li, Q. Sun, F. Han, D.-H. Liu, Y. Guo, *Angew. Chem. Int. Ed.* **2011**, *50*, 11765.
3. J. Liu, S. Z. Qiao, H. Liu, J. Chen, A. Orpe, D. Zhao, G. Q. Lu, *Angew. Chem. Int. Ed.* **2011**, *50*, 5947.
4. S. Wang, W. C. Li, G. P. Hao, Y. Hao, Q. Sun, X. Q. Zhang, A. H. Lu, *J. Am. Chem. Soc.* **2011**, *133*, 15304.
5. B. Hu, Y. Zhao, H. Z. Zhu, S.-H. Yu, *Acs Nano* **2011**, *5*, 3166.
6. S. R. Guo, J. Y. Gong, P. Jiang, M. Wu, Y. Lu, S. H. Yu, *Adv. Funct. Mater.* **2008**, *18*, 872.
7. A. T. Rodriguez, X. Li, J. Wang, W. A. Steen, H. Fan, *Adv. Funct. Mater.* **2007**, *17*, 2710.
8. K. Ai, Y. Liu, C. Ruan, L. Lu, G. Lu, *Adv. Mater.* **2013**, *25*, 998.
9. X. W. Lou, C. M. Li, L. A. Archer, *Adv. Mater.* **2009**, *21*, 2536.
10. Y. H. Ng, S. Ikeda, T. Harada, S. Higashida, T. Sakata, H. Mori, M. Matsumura, *Adv. Mater.* **2007**, *19*, 597.
11. R. Liu, S. M. Mahurin, C. Li, R. R. Unocic, J. C. Idrobo, H. Gao, S. J. Pennycook, S. Dai, *Angew. Chem. Int. Ed.* **2011**, *50*, 6799.
12. M. M. Titirici, M. Antonietti, *Chem. Soc. Rev.* **2010**, *39*, 103.
13. D. S. Su, R. Schlogl, *ChemSusChem* **2010**, *3*, 136.
14. M. Kim, K. Sohn, H. Bin Na, T. Hyeon, *Nano Lett.* **2002**, *2*, 1383.
15. Y. Shi, Y. Wan, D. Zhao, *Chem. Soc. Rev.* **2011**, *40*, 3854.
16. T. Ma, L. Liu, Z. Yuan, *Chem. Soc. Rev.* **2013**, *42*, 3977.
17. D. Gu, F. Schueth, *Chem. Soc. Rev.* **2014**, *43*, 313.
18. Y. Deng, J. Wei, Z. Sun, D. Zhao, *Chem. Soc. Rev.* **2013**, *42*, 4054.
19. C. Liang, Z. Li, S. Dai, *Angew. Chem. Int. Ed.* **2008**, *47*, 3696.
20. Y. Zhai, Y. Dou, D. Zhao, P. F. Fulvio, R. T. Mayes, S. Dai, *Adv. Mater.* **2011**, *23*, 4828.
21. A. Stein, Z. Wang, M. A. Fierke, *Adv. Mater.* **2009**, *21*, 265.
22. Y. Fang, D. Gu, Y. Zou, Z. Wu, F. Li, R. Che, Y. Deng, B. Tu, D. Zhao, *Angew. Chem. Int. Ed.* **2010**, *49*, 7987.
23. J. Choma, D. Jamiola, K. Augustynek, M. Marszewski, M. Gao, M. Jaroniec, *J. Mater. Chem.* **2012**, *22*, 12636.
24. A. B. Fuertes, P. Tartaj, *Small* **2007**, *3*, 275.
25. T. W. Kim, P. W. Chung, I. I. Slowing, M. Tsunoda, E. S. Yeung, V. S. Y. Lin, *Nano Lett.* **2008**, *8*, 3724.
26. H. J. Liu, W. J. Cui, L. H. Jin, C. X. Wang, Y. Y. Xia, *J. Mater. Chem.* **2009**, *19*, 3661.
27. J. Gu, S. Su, Y. Li, Q. He, J. Shi, *Chem. Commun.* **2011**, *47*, 2101.
28. J. Schuster, G. He, B. Mandlmeier, T. Yim, K. T. Lee, T. Bein, L. F. Nazar, *Angew. Chem. Int. Ed.* **2012**, *51*, 3591.
29. J. Liu, T. Yang, D.-W. Wang, G. Q. Lu, D. Zhao, S. Z. Qiao, *Nature Commun.* **2013**, *4,* 2798.
30. Z.-A. Qiao, B. Guo, A. J. Binder, J. Chen, G. M. Veith, S. Dai, *Nano Lett.* **2013**, *13*, 207.
31. Z. Sun, Y. Liu, B. Li, J. Wei, M. Wang, Q. Yue, Y. Deng, S. Kaliaguine, D. Zhao, *Acs Nano* **2013**, *7*, 8706.
32. Z. Wu, W. D. Wu, W. Liu, C. Selomulya, X. D. Chen, D. Zhao, *Angew. Chem. Int. Ed.* **2013**, *52*, 13764.
33. Y. Fang, G. Zheng, J. Yang, H. Tang, Y. Zhang, B. Kong, Y. Lv, C. Xu, A. M. Asiri, J. Zi, F. Zhang, D. Zhao, *Angew. Chem. Int. Ed.* **2014**, *53*, 5366.
34. A. H. Lu, F. Schüth, *Adv. Mater.* **2006**, *18*, 1793.
35. Z. Wang, F. Li, A. Stein, *Nano Lett.* **2007**, *7*, 3223.
36. J. E. Hampsey, Q. Y. Hu, L. Rice, J. B. Pang, Z. W. Wu, Y. F. Lu, *Chem. Commun.* **2005**, 3606.
37. A. B. Fuertes, *J. Mater. Chem.* **2003**, *13*, 3085.
38. J. Ren, J. Ding, K. Y. Chan, H. Wang, *Chem. Mater.* **2007**, *19*, 2786.
39. Y. D. Xia, R. Mokaya, *Adv. Mater.* **2004**, *16*, 886.
40. Y. Meng, D. Gu, F. Q. Zhang, Y. F. Shi, H. F. Yang, Z. Li, C. Z. Yu, B. Tu, D. Y. Zhao, *Angew. Chem. Int. Ed.* **2005**, *44*, 7053.
41. C. D. Liang, S. Dai, *J. Am. Chem. Soc.* **2006**, *128*, 5316.
42. C. D. Liang, K. L. Hong, G. A. Guiochon, J. W. Mays, S. Dai, *Angew. Chem. Int. Ed.* **2004**, *43*, 5785.
43. F. Q. Zhang, Y. Meng, D. Gu, Y. Yan, C. Z. Yu, B. Tu, D. Y. Zhao, *J. Am. Chem. Soc.* **2005**, *127*, 13508.
44. S. Tanaka, N. Nishiyama, Y. Egashira, K. Ueyama, *Chem. Commun.* **2005**, 2125.
45. J. Wei, D. Zhou, Z. Sun, Y. Deng, Y. Xia, D. Zhao, *Adv. Funct.Mater.* **2013**, *23*, 2322.
46. J. Wei, Y. H. Deng, J. Y. Zhang, Z. K. Sun, B. Tu, D. Y. Zhao, *Solid State Sci.* **2011**, *13*, 784.
47. D. Gu, H. Bongard, Y. Meng, K. Miyasaka, O. Terasaki, F. Zhang, Y. Deng, Z. Wu, D. Feng, Y. Fang, B. Tu, F. Schüth, D. Zhao, *Chem. Mater.* **2010**, *22*, 4828.
48. X. Wang, C. Liang, S. Dai, *Langmuir* **2008**, *24*, 7500.
49. Q. S. Huo, D. I. Margolese, U. Ciesla, P. Y. Feng, T. E. Gier, P. Sieger, R. Leon, P. M. Petroff, F. Schüth, G. D. Stucky, *Nature* **1994**, *368*, 317.
50. M. K. Debe, *Nature*, **2012**, *486*, 43.
51. Q. Li, R. Cao, J. Cho, G. Wu, *Adv. Energy. Mater.* **2014**, *4*, 1301415.
52. Y. Zheng, Y. Jiao, M. Jaroniec, Y. Jin, S. Z. Qiao, *Small* **2012**, *8,* 3550.
53. G. Wu, P. Zelenay, *Acc. Chem. Res.* **2013**, *46*, 1878.
54. S. Guo, S. Zhang, S. Sun, *Angew. Chem. Int. Ed.* **2013**, *52*, 8526.
55. D. Wang, D. Su, *Energy Environ. Sci.*, **2014**, *7*, 576.
56. B. Xia, Y. Yan, X. Wang, X. Lou, *Mater. Horiz.*, **2014**, *1*, 379.
57. B. Xia, J. Wang, X. Wang, J. Niu, Z. Sheng, M. Hu, Q. Yu, *Adv. Funct. Mater.* **2008**, *18*, 1790.